© 2019. Published by The Company of Biologists Ltd | Journal of Cell Science (2019) 132, jcs231563. doi:10.1242/jcs.231563

RESEARCH ARTICLE

Circulating tumor cells exit circulation while maintaining multicellularity, augmenting metastatic potential

Tyler A. Allen[1], Dana Asad[2], Emmanuel Amu[1], M. Taylor Hensley[1], Jhon Cores[1,2], Adam Vandergriff[1,2], Junnan Tang[3], Phuong-Uyen Dinh[1], Deliang Shen[1], Li Qiao[1], Teng Su[2], Shiqi Hu[1], Hongxia Liang[1], Heather Shive[1], Erin Harrell[1], Connor Campbell[1], Xinxia Peng[1,4,5], Jeffrey A. Yoder[1] and Ke Cheng[1,2,*]

ABSTRACT

Metastasis accounts for the majority of all cancer deaths, yet the process remains poorly understood. A pivotal step in the metastasis process is the exiting of tumor cells from the circulation, a process known as extravasation. However, it is unclear how tumor cells extravasate and whether multicellular clusters of tumor cells possess the ability to exit as a whole or must first disassociate. In this study, we use *in vivo* zebrafish and mouse models to elucidate the mechanism tumor cells use to extravasate. We found that circulating tumor cells exit the circulation using the recently identified extravasation mechanism, angiopellosis, and do so as both clusters and individual cells. We further show that when melanoma and cervical cancer cells utilize this extravasation method to exit as clusters, they exhibit an increased ability to form tumors at distant sites through the expression of unique genetic profiles. Collectively, we present a new model for tumor cell extravasation of both individual and multicellular circulating tumor cells.

This article has an associated First Person interview with the first author of the paper.

KEY WORDS: Angiopellosis, Circulating tumor cell cluster, Tumor cell extravasation, Cancer exodus hypothesis, Metastasis

INTRODUCTION

Metastasis remains the leading cause of cancer-related deaths worldwide (Anderson et al., 2018). It is a complex process involving tumor cell invasion from the primary site, intravasation into the circulation, and their extravasation (exiting) from vessels at distant sites. The molecular mechanisms regulating this process are poorly understood, but it is clearly dependent on ability of the tumor cells to transmigrate the blood vessel wall. Only a small percentage of all tumor cells ever successfully make this journey, and even fewer actually survive following extravasation to form secondary tumors. Recently, it has been discovered certain adult non-leukocytic cells possess the ability to extravasate through a novel mechanism, known as angiopellosis (AP) (Allen et al., 2017), which involves the restructuring of the vascular wall around the circulating cells, and the active expulsion of these cells from the lumen to the surrounding tissue. The AP mechanism is distinct from diapedesis and was shown to allow for the extravasation of both individual cells and multicellular clusters, without the need for the clusters to disassociate prior to extravasation.

Accumulating data suggests that metastatic primary tumor cells disseminate through the circulation and seed at distant sites as multicellular clusters (Aceto et al., 2014, 2015; Stott et al., 2010). However, the method these circulating tumor cell clusters use to exit circulation and whether they must first dissociate prior to remains unknown (Miles et al., 2008; Gassmann et al., 2009). Circulating tumor cell (CTC) clusters make up only a small percentage of CTCs but have been shown to have increased metastatic potential and correlate to poor prognosis in cancer patients. Recent studies have shown CTC clusters have the ability to travel through circulation, and seed at metastatic sites while maintaining adherence, but it is unknown how the clusters are extravasating (Au et al., 2016). We hypothesized that CTCs possess the ability to extravasate through AP as both individual cells and clusters, and the number of extravasating cells affects the ability of the tumor cells to form distant tumors.

Limitations on the ability to image CTCs in circulation have hindered progress on fully understanding the complexity of the metastasis process. Here, by studying metastasis using an *in vivo* zebrafish embryo/larvae model, we demonstrate CTC clusters possess the ability to exit blood vessels both as single cells and multicellular clusters through the recently identified AP method of extravasation (Allen et al., 2017). Additionally, we found cervical and melanoma tumor cells that extravasate as multicellular clusters through AP exhibit an augmented ability to proliferate, while individually extravasating cells remain dormant at a higher frequency. These extravasating tumor cells exhibit unique dysregulation of certain genes, which aids in their ability to exit vessels and seed at distant sites, through cell adhesion-mediated modulation of binding factors on both CTCs and endothelial cells. Our results challenge the prevailing notion CTC clusters must first disassociate to exit the circulation and posits an alternative model (Strell et al., 2008). We propose tumor cells can both travel though and exit the circulation while maintaining a multicellular phenotype, and the ability of CTC clusters to extravasate as a whole through AP contributes to their increased rates of secondary tumor formation in patients by allowing them to preserve the CTC cluster microenvironment at a distant site. We anticipate our findings to provide a starting point for more complex *in vivo* studies understanding the dynamics of group extravasation on tumor cluster's ability to establish secondary tumors at distant sites.

RESULTS

CTCs extravasate mainly through AP

To characterize the extravasation mechanism of tumor cells *in vivo*, 20–30 fluorescent human cervical (HeLa) tumor cells were infused

[1]Department of Molecular Biomedical Sciences and Comparative Medicine Institute, North Carolina State University, Raleigh, NC 27607, USA. [2]Joint Department of Biomedical Engineering, University of North Carolina at Chapel Hill and North Carolina State University, Chapel Hill, NC 27607, USA. [3]Department of Cardiology, The First Affiliated Hospital of Zhengzhou University, Zhengzhou, Henan 450001, China. [4]Bioinformatics Research Center, North Carolina State University, Raleigh, NC 27607, USA. [5]Bioinformatics Graduate Program, North Carolina State University, Raleigh, NC 27607, USA.

*Author for correspondence (kcheng3@ncsu.edu)

T.A.A., 0000-0002-8729-6339; M.T.H., 0000-0002-7202-2116; D.S., 0000-0002-1826-5141; L.Q., 0000-0002-6372-7157; H.L., 0000-0002-3229-1426

Received 4 March 2019; Accepted 25 July 2019

Journal of Cell Science (2019) 132, jcs231563. doi:10.1242/jcs.231563

directly into the circulation of tg(*fli1a*:egfp) zebrafish, which possess fluorescent blood vessels (Fig. 1A) (Blum et al., 2008). Following infusion, HeLa cells were tracked through intravital lightsheet microscopy, for up to 24 h, to visualize the extravasation process in real-time. HeLa cells exited blood vessels through both the recently identified angiopellosis (AP) mechanism of extravasation, and the canonical diapedesis mechanism (Fig. 1B,C). The AP method characteristically elicited remodeling of the endothelial cells (indicated by the yellow dotted line), and actively expelled the HeLa cells from the lumen into the surrounding tissue (Fig. 1B; Movie 1). In contrast, when HeLa cells underwent diapedesis through the characteristic penetration of the endothelial wall, there were only

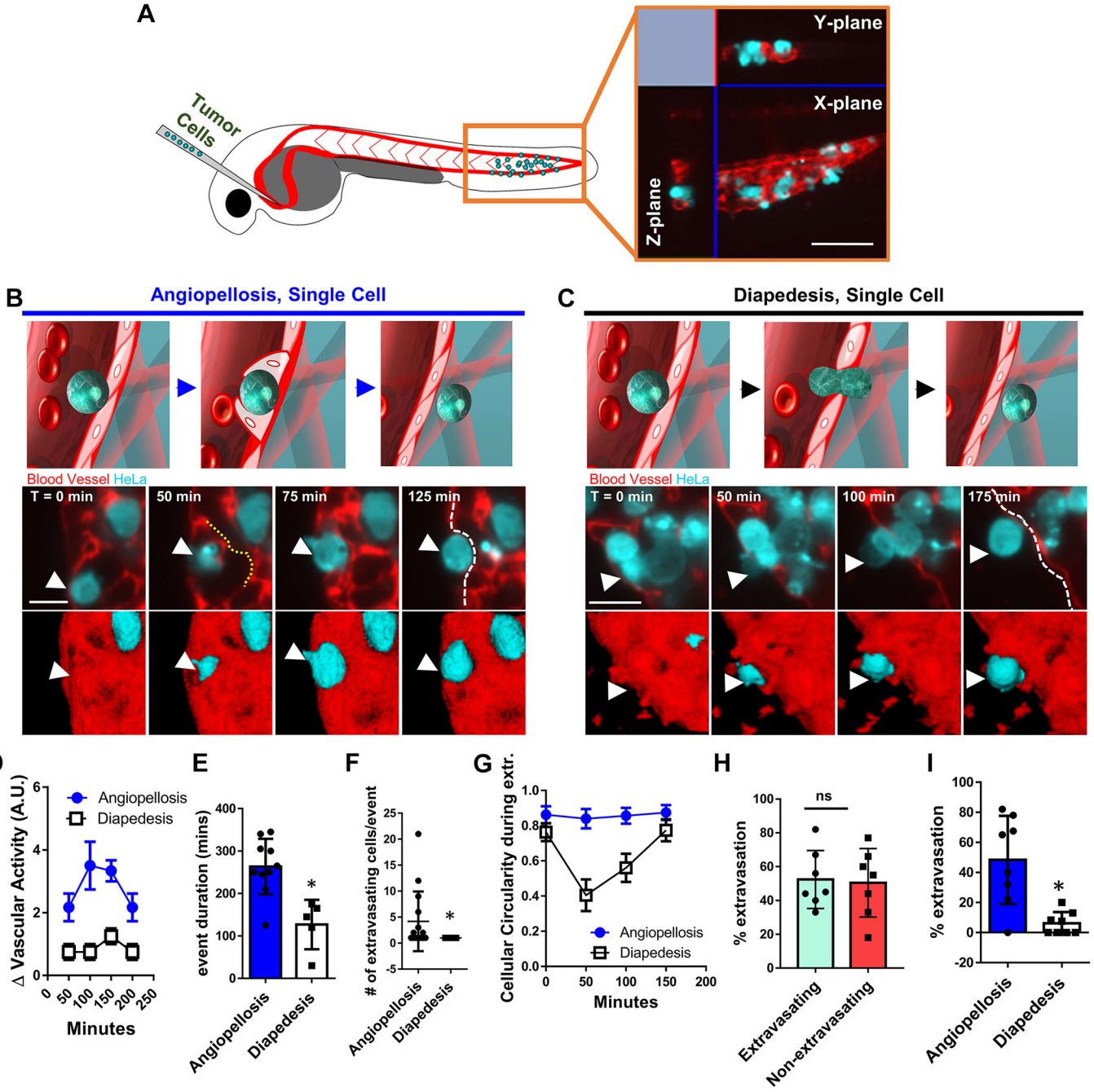

Fig. 1. Human cervical cancer cells possess the ability to extravasate blood vessels through both AP and diapedesis. (A) Illustration of the injection of fluorescent tumor cells into the circulation of zebrafish embryos. Scale bar: 200 µm. (B) Representative time lapse images of a HeLa cell (cyan) undergoing extravasation to exit blood vessels (red) through AP; the yellow dotted line indicates vascular remodeling; the white dashed line indicates the border of the outermost portion of the blood vessel. Scale bar: 20 µm. (C) Representative time lapse images of a HeLa cell (cyan) undergoing extravasation to exit blood vessels (red) through diapedesis. Scale bar: 20 µm. Arrowheads highlight the position of the extravasating tumor cell. (D–F) Graphical representation of the vascular activity of the vessel during extravasation, the duration of the extravasation events and the number of cells which exited during each extravasation event; data is representative of at least n=4 injected zebrafish, and n=30 for tumor cells (multiple extravasation events occur in each zebrafish). (G–I) Graphical representation of the circularity of tumor cells during the extravasation events, the percentage of cells that extravasated the vessels, and the percentage of cells which exited through AP or diapedesis; data is representative of at least n=4 injected zebrafish, and n=30 for tumor cells. *P<0.05; ns, not significant. A.U., arbitrary units.

Journal of Cell Science

Journal of Cell Science (2019) 132, jcs231563. doi:10.1242/jcs.231563

low levels of vascular remodeling (Fig. 1C; Movie 2). The movement of endothelial cells during this process was tracked/measured as vascular activity, which revealed cells undergoing AP empirically elicited higher rates of vascular remodeling (Fig. 1D). On average, the tumor cells required 136.5 min longer to undergo a complete AP extravasation event, compared to the tumor cells undergoing diapedesis (P<0.01), with the average duration for the AP extravasation events being 263.5 min, and 127 min for diapedesis (Fig. 1E). We observed that multiple tumor cells were able to exit vessels simultaneously through AP, while only individual cells were observed to extravasate through diapedesis (Fig. 1F). Interestingly, tumor cells which extravasated through diapedesis were observed to exit exclusively as individual cells, even when travelling in circulation as clusters. Another distinction observed between the two methods was the change in cell circularity during the extravasation events. Tumor cells undergoing diapedesis exhibited a dumbbell shape and they squeezed through the endothelial wall, while cells undergoing AP retained their circularity while undergoing the event (Fig. 1G; Movie 5). Of the 20–30 cells infused, 49.66% extravasated into the surrounding tissue, with the others remaining inside the lumen over the course of the 24-h observation (Fig. 1H). Nearly 15 times more HeLa cells exited through AP (46.5%), than the diapedesis method (3.16%), suggesting AP as the leading extravasation mechanism in this model (Fig. 1I).

AP supports cancer cluster extravasation

To evaluate the extravasation behavior of multicellular CTC clusters, we injected high-density amounts of tumor cells (50–60) to stimulate cell clustering in circulation (preclustered cell aggregates are too large to inject). Tumor cell clusters were observed to exit while maintaining multicellularity (cluster phenotype without disassociation) through AP, adding to the differences observed between AP and diapedesis (Fig. 2A,B). Specifically, we observed HeLa cells that formed clusters *in vivo* possessed the ability to exit blood vessels as clusters, through AP, into the surrounding tissue and extravascular cavities (Fig. 2C; Movie 3). This phenomenon was also observed in ZF3 primary cancer cells derived from a tumor isolated from an adult transgenic tg($brca2^{hg5}$/$tp53^{zdf1}$) mutant zebrafish, and

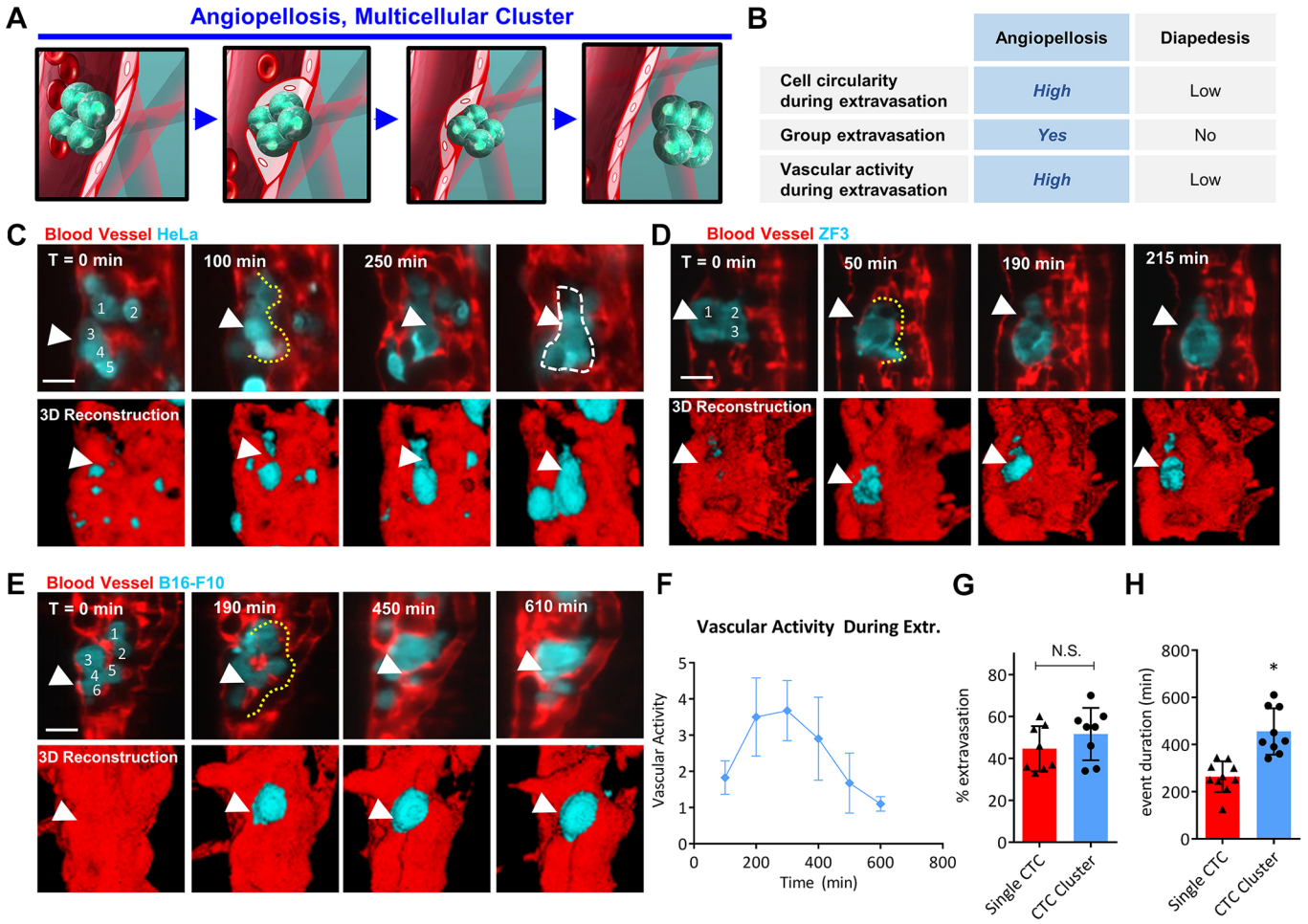

Fig. 2. Human cervical cancer and melanoma tumor cell clusters exit as multicellular aggregates through AP. (A) Illustration of a tumor cell cluster (cyan) undergoing extravasation of a blood vessel (red) though AP. (B) Table listing key differences observed in tumor cell extravasation through AP and diapedesis. (C) Representative time lapse images of a HeLa cell cluster (cyan) undergoing extravasation to exit blood vessels (red) through AP; the yellow dotted line indicates vascular remodeling; the white dashed line indicates the border of the extravascular cavity the tumor cells extravasated into. Scale bar: 20 µm. (D) Representative time lapse images of a ZF3 zebrafish primary tumor cell cluster (cyan) undergoing extravasation to exit blood vessels (red) through AP; the yellow dotted line indicates vascular remodeling. Scale bar: 20 µm. (E) Representative time lapse images of a B16F10 cell cluster (cyan) undergoing extravasation to exit blood vessels (red) through AP; yellow dotted line indicates vascular remodeling. Numbers denote individual cells. Arrowheads highlight the position of the extravasating tumor cell. Scale bar: 20 µm. (F,G) Graphical representation of vascular activity (in arbitrary units) of tumor cell clusters during the AP extravasation, and the percentage of CTCs which exited as single cells or multicellular clusters; n=8. (H) Graphical representation of the duration of the events of CTC clusters and single CTCs; n=10. *P<0.05; N.S., not significant.

Journal of Cell Science

Journal of Cell Science (2019) 132, jcs231563. doi:10.1242/jcs.231563

infused metastatic murine melanoma (B16F10) cells (Fig. 2D,E). Similar to the AP extravasation events observed for single tumor cells, the tumor cell clusters elicited increased vascular activity during the process (Fig. 2F). Although, the percentage of single CTCs and clustered CTCs that successfully extravasated was not significantly different (P=0.536; Fig. 2G) the duration of time it took for the AP process to complete was significantly (P<0.01) longer in CTC clusters (Fig. 2H). No CTC clusters were observed to utilize diapedesis to extravasate while maintaining multicellularity. However, single cells from CTC clusters did show the ability to separate from the cluster and extravasate through diapedesis as individual cells (Movie 4).

Tumor cell cluster extravasation leads to higher metastatic potential

Although CTC clusters did not show an increased occurrence of extravasation compared to single CTCs (Fig. 2G), studies have linked the presence of CTC clusters in the blood to poor patient outcomes leading us to investigate other qualities of CTC clusters that could potentially contribute to poor prognosis (Duda et al., 2010; Huang et al., 2016). Since diapedesis only allows for a single cell to leave, we further investigated the role of AP in CTC cluster tumor formation following extravasation. We infused HeLa and B16F10 tumor cells in either high or low density concentrations to induce cluster extravasation or single-cell extravasation in circulation. We then followed the fate of CTCs for up to 96 h following extravasation out of the blood vessel(s). HeLa cells that extravasated as isolated single cells through either AP or diapedesis did not proliferate over the 96 h, but maintained their fluorescence intensity levels, implicating viability (Fig. 3A,B). However, HeLa and B16F10 tumor cells that exited as clusters (>2 cells), through AP, exhibited higher proliferative capability (Fig. 3C,D; Movies 6 and 7). Tumor cell growth was measured and showed an increase over the 96 h following extravasation for tumor clusters in both HeLa and B16f10 cells (Fig. 3E). Of note, 0% of the tumor cells that extravasated as single cells through either AP or diapedesis were observed to proliferate over the course of 4 days, in comparison to 92.5% of CTC clusters showing proliferation following extravasation (Fig. 3F).

To determine whether cluster extravasation increased tumor formation in a mammalian model, we infused equivalent amounts (300,000; calculated based on murine vessel size relative to zebrafish vasculature) of luciferase-expressing B16F10 and A375 melanoma cells into C57BL/6J and NSG-SCID mice, respectively, as either prepared clusters or dissociated individual cells (Fig. 3G) and observed the lung tumor formation through bioluminescence imaging (Fig. 3H). The B16F10 cells infused as clusters (B16F10-cluster) exhibited an increased ability to form tumors in the lung compared to the B16F10s infused as disassociated (B16F10-diss) and single (B16F10-sing) cells (Fig. 3I–K), correlating with the increased tumor formation of clusters observed in the zebrafish imaging. This occurrence was validated in NSG-SCID mice, with A375 cells infused as clusters exhibiting increased tumor formation in the lungs, compared to equivalent amounts of A375 cells infused as non-clustered disassociated cells (Fig. 3L–N). Immunohistochemistry staining of C57BL/6J lungs following infusion of fluorescent B16F10 tumor cells clusters showed intact multicellular clusters in the lungs after only 8 h post infusion (hpi) (Fig. 3O). This suggests that CTCs maintain the ability to exit vessels as clusters through AP in mammalian vasculature, which may be a contributing factor to their increased ability to form tumors at distant sites in cancer patients. These data strengthen conclusions from studies reporting increased tumor seeding capabilities when in clusters, and suggest that tumor cells that exit while maintaining their multicellularity not only have an increased ability to survive metastasis but maintain a distinct proliferation advantage when compared to individually extravasating tumor cells (Aceto et al., 2014; Au et al., 2016).

AP-associated genes and molecular pathways

Since not all tumor cells observed in circulation ever extravasate and proliferate (Fig. 1H), we set out to further characterize the extravasation-positive subset of CTCs to investigate their uniqueness at the genetic level. Florescent B16F10 cells infused into zebrafish that extravasated as clusters through AP (termed B16Met cells) were isolated from zebrafish and cultured *in vitro* to establish a stable sub-line for downstream analysis. Transcriptome analysis (RNA sequencing) of B16Met cells revealed differential gene expression of 1955 genes compared to the parental B16F10 line (Fig. 4A; Table S1) including the cell-adhesion related subset: *MCAM*, *COL1A*, *ITGA1*, *ADAMTS12* and *PCDHB16* (Fig. 4B). Ingenuity pathway analysis (IPA) of the B16Met cell line also showed differentially regulated genes that were significantly involved in both PTEN and integrin signaling pathways (Figs S1, S2). To examine the biological and clinical relevance of the gene expression of B16Met cells, we compared the gene expression in these cells to that in cells from melanoma patients as described in the The Cancer Genome Atlas (TCGA) (Gundem et al., 2010). The aforementioned adhesion-related genes exhibit expression in the majority of TCGA melanoma patient tumor samples, and when patient data was divided based on level of expression (either High or Low), survival analysis showed significant (P<0.05) correlation between mRNA expression level and patient survival. This suggests that the B16Met sub-line may share similar characteristics to CTC clusters in melanoma patients, and that the dysregulation of key adhesion-related genes in tumor cells is a potential factor contributing to their extravasation and proliferation potential (Glinskii et al., 2005).

We further studied the metastatic potential of the B16Met subset through the reintroduction into the zebrafish circulation. Intravital microscopy revealed that B16Met cells exhibited an increased ability to extravasate through AP as clusters compared to control B16F10 cells (Fig. 4C,D). To further validate biological relevance in a mammalian model, we tested the metastatic potential of the B16Met cells in comparison to B16F10 control cells, in a syngeneic mouse infusion model. B16Met and B16F10 cell lines were used, and 7×10^5 cells were intravenously infused into C57BL/6J mice through tail-vein infusion (Fig. 4E). After 10 days, we collected the lung tissue. We observed that mice infused with B16Met cells showed a significant (P<0.05) increase in the number of metastatic nodules displayed in the lungs, in comparison to control B16f10 cells (Fig. 4F,G). This suggests AP-extravasating tumor sub-lines maintain/possess unique characteristics that allow for preferential CTC cluster extravasation through AP and thus an increased potential to form distant tumors.

Molecular characterization of AP-participating endothelial and tumor cells

To gain deep mechanistic insight into the mediators involved in AP extravasation, we developed an *in vivo* model using the photoactivatable GFP-to-RFP fluorescence protein EosFP to isolate extravasation-participating tumor and endothelial cells immediately following extravasation for downstream analysis. The tg(*kdrl:tdEos2*)*ubs15* zebrafish line, with exclusive expression of EosFP in endothelial cells, was infused with florescent human melanoma

Journal of Cell Science (2019) 132, jcs231563. doi:10.1242/jcs.231563

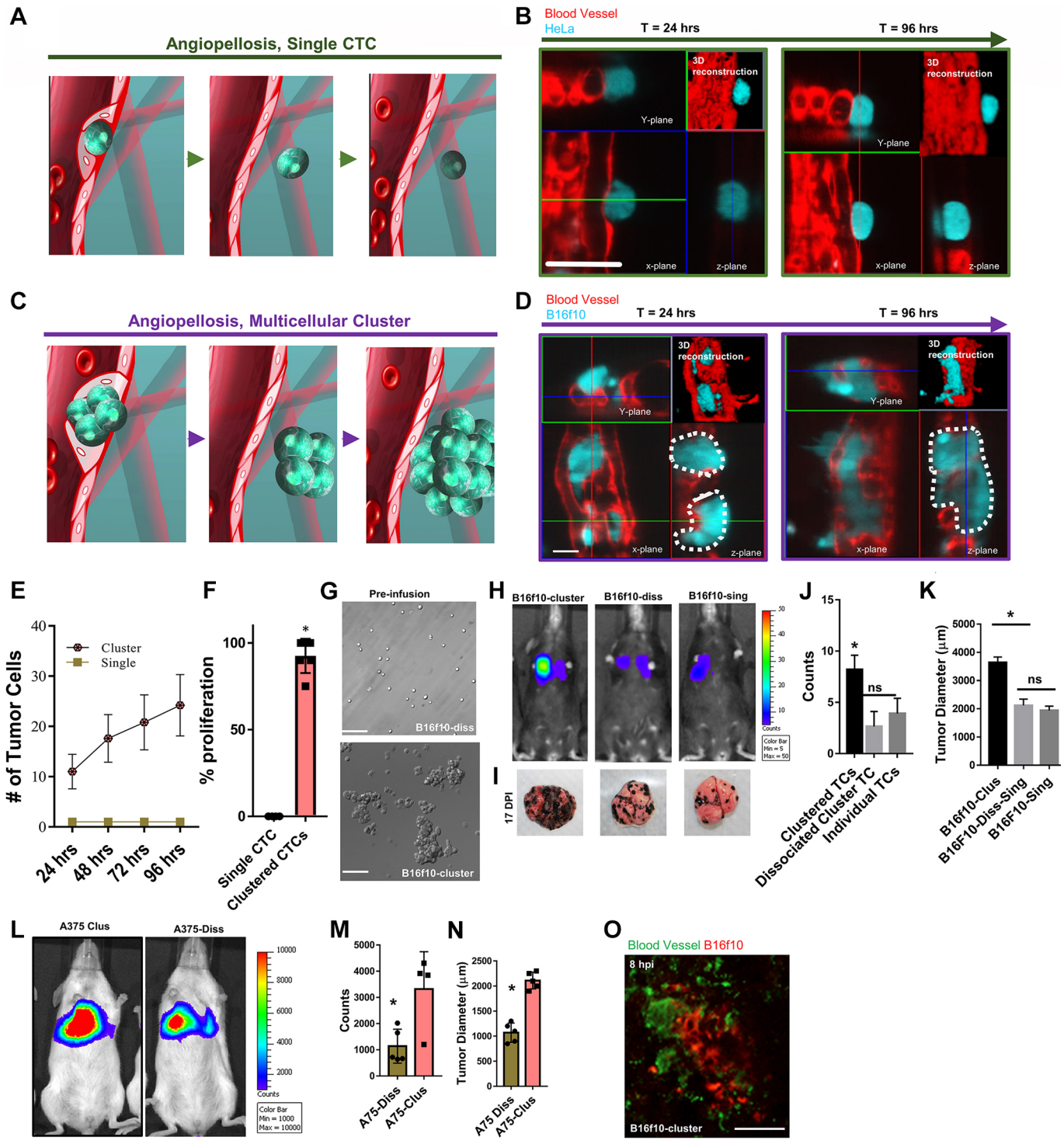

Fig. 3. See next page for legend.

(A375) cells (Lenard et al., 2013). Immediately following CTC cluster extravasation through AP, the extravasation-participating endothelial cells were photoactivated through targeted Ultra Violet emission and sorted through fluorescence-activated cells sorting (FACS) (Fig. 5A). Transcriptome analysis in these cells revealed 2416 differentially expressed genes (DEGs), with the top 30 containing several genes with human-zebrafish orthologs including: *VIMR1, STC2B, LUM* and *TYRP1B* (Fig. 5A; Table S3). Additionally, analysis of signal pathways through IPA revealed that there was dysregulation of both the tight junction and aryl hydrocarbon receptor signal pathways (Figs S3, S4). Additionally, Gene Ontology (GO) terms were enriched for both cell adhesion and ion transport (Fig. 5C). This suggests CTC–endothelial cell interaction may directly modulate the cell adhesion and ion transport signal transduction pathways of endothelial cells, prompting the AP extravasation mechanism to occur.

Next, to further investigate the molecular players involved in CTC cluster extravasation through AP, we stably transduced A375 cells to express EosFP (termed A375-EOS) and infused them

Journal of Cell Science (2019) 132, jcs231563. doi:10.1242/jcs.231563

Fig. 3. Circulating tumor cells which exit vessels as clusters show augmented proliferation ability. (A) Illustration of a single tumor cell (cyan) extravasating a blood vessel and remaining dormant (non-proliferative). (B) Representative orthographic time lapse images of a single HeLa cell (cyan) following extravasation at 24 h post injection, then an image of the same cell at 96 h post injection. Scale bar: 20 µm. (C) Illustration of clustered tumor cells (cyan) extravasating from a blood vessel (red) and showing proliferation capability. (D) Representative orthographic time lapse images of a single HeLa cell cluster (cyan) following extravasation at 24 h post injection, then an image of the same cluster at 96 h post injection. Scale bar: 20 µm. White dotted lines highlight the outline of the tumor cell cluster following AP extravasation. (E) Graphical representation of the number of tumor cells found owing to proliferation following extravasation of either CTC clusters or single CTCs (n=10). (F) Graph of the percentage of single or clustered CTCs that, following extravasation, proliferated *in vivo* over the 96-h observation period (n=10). (G) Representative images of B16F10 cells as either disassociated cells (top) or clusters (bottom) prior to infusion into mice through tail vein. Scale bars: 200 µm. (H,I) Representative images of C57BL/6J mice imaged after 10 dpi using bioluminescent imaging to determine the relative amount of metastasis (color coding from blue to red) in the lungs; mice received 300,000 B16F10-luciferase cells cultured as clusters, cells cultured as clusters and dissociated prior to infusion, and cells cultured as non-clustered single cells. (J,K) Graphs representing the bioluminescence counts of the tumors forming in the mice from the respective groups, and the diameter of the tumors from histological examination of the respective mice lungs (n=4). (L) Representative image of NSG-SCID mice infused with either clustered A375 cells (A375-clus) or individual disassociated A375 cells (A375-Diss); n=4. (M,N) graphical representation of the bioluminescence counts and tumor diameter of the histological examination of the lung. (O) Representative immunohistochemistry section of C57BL/6J mice lungs 8 h post infusion of B16F10 clusters; staining is for endothelial cells (blood vessel) using anti-Von Willebrand factor (vWF) and B16F10 cells using anti-Melanoma gp100 antibodies. Scale bar: 20 µm. *P<0.05; ns, not significant.

into circulation of tg(*fli1a:egfp*) zebrafish. Immediately following observed extravasation through AP, the A375-EOS cells that extravasated as cluster were photoactivated and isolated through FACS for analysis using ultra-low input RNAseq (Fig. 5B; Table S2). Transcriptome (RNA-seq) analysis of these extravasating A375-EOS cell clusters revealed significant differential gene expression of 3337 genes compared to non-infused control A375-EOS cells. Of the identified differentially expressed genes, 214 were also differentially regulated in the B16Met line (Fig. S5A). Additionally, of the top 20 protein-coding genes differentially expressed in the A375-EOS cells, seven had significant (P<0.05) correlation between mRNA expression level and patient survival in the TCGA melanoma patient samples. This suggests the subset of genes differentially expressed in certain CTC populations may allow these tumor cells to undergo AP more effectively, which correlates to an increase in metastatic ability.

DISCUSSION

The limitations of current imaging technologies prevent the intravital imaging of tumor cell extravasation in real time in humans, but the zebrafish offers a biologically relevant system to deeply study key aspects of this process (Bradford et al., 2017; Ablain and Zon, 2013; Gore et al., 2012; Chávez et al., 2016). Taking advantage of a model that allows for the visualization of tumor cells extravasation in real time, and a unique method to isolate extravasation-participating tumor and endothelial cells, we show that CTCs possess the ability to extravasate through AP by triggering the activation of vascular remodeling in endothelial cells. Furthermore, we show that multicellular CTC clusters utilize AP to exit without first disassociating, giving them an augmented ability to form tumors at distant sites. Our results point to AP as the main mechanism used by CTCs to extravasate, and the only observed mechanism to allow for CTC clusters to extravasate while maintaining their multicellularity. Previous studies have shown that CTC clusters have distinct survival and secondary tumor formation abilities, but these studies were limited in their ability to characterize how the CTC clusters were exiting blood vessels (Aceto et al., 2014, 2015; Stott et al., 2010). This limitation hindered the ability to fully understand the importance of how multicellularity of CTC clusters impacts the ability of tumor cells to spread to distant areas of the body. Our findings provide novel insight on the ability of CTC clusters to travel through circulation as well as how the varying mechanisms of extravasation influence tumor progression at distant sites.

We have shown that CTCs attach to the blood vessel lumen and, through cell adhesion molecule-mediated binding, activate vascular remodeling, which allows them to escape into the surrounding tissues as either single cells or multicellular clusters. Studies have shown that CTCs are faced with the loss of integrin-facilitated anchorage to the extracellular matrix, making them susceptible to anoikis-mediated apoptosis (Taddei et al., 2012). The formation of multicellular clusters is used by metastatic tumor cells to avoid anoikis but inhibits the ability of CTCs to travel through the endothelial wall in a diapedesis-like manner (Hou et al., 2011). In contrast to these previous studies, our results demonstrate that CTCs possess the ability to exit through both diapedesis as well as the recently identified mechanism of AP, and the unique genetic profiles of this subset of CTCs gives them an increased ability to prompt the extravasation process. A point to consider for subsequent studies include characterization of AP-extravasating cells beyond the gene expression level (morphological, biochemical and DNA methylation characterization), and this effect on extravasation.

Although AP extravasation was first discovered to be utilized by adult non-leukocytic stem cells, it was unknown whether tumor cells possessed a similar ability to prompt the vascular remodeling necessary for the process to occur. Our results show that not only were individual CTCs able to utilize AP, but multicellular CTC clusters could prompt the AP mechanism allowing for clusters to extravasate, challenging the notion that CTC clusters must disassociate prior to extravasation. Our model uses an artificial infusion of tumor cells to study the extravasation portion of metastasis, but further studies using this type of intravital imaging techniques to study the invasion and dissemination process are needed to fully understand the role of vasculature, CTCs and CTC clusters in metastasis. Additionally, studies focusing on the impact of manipulating the conditions of inocula prior to infusion will be of interest in further understanding the pre-extravasation role of CTCs in the process of metastasis.

Previous studies using *in vivo* Na^+/K^+ ATPase inhibitors have shown that hypomethylation of binding sites for the TFs OCT4, SOX2, NANOG and SIN3A are found in CTC clusters, and dissociation caused the reversal of the methylation profiles of CTCs and suppressed their metastasis (Gkountela et al., 2019). However, in the present study, we have shown the dissociation of CTC clusters was not required for extravasation and the seeding at distant sites, and that CTC cluster disassociation caused suppression of metastatic tumor formation in both zebrafish and mice, but not suppression of tumor extravasation itself. Our results also show the dysregulation of specific genes/pathways from isolated extravasation-participating tumor and endothelial cells directly correlated to the potential of the CTCs to undergo extravasation and tumor formation at distant sites. Interestingly, the profiles of both human and murine extravasation-positive CTCs showed a noteworthy amount of overlapping gene sets, suggesting conservation of AP-extravasation-contributing molecules found in cancer cells. Previous studies have shown a positive correlation exists between increased homotypic adhesion and experimental metastatic potential (Updyke et al., 1986; Urushihara

Journal of Cell Science (2019) 132, jcs231563. doi:10.1242/jcs.231563

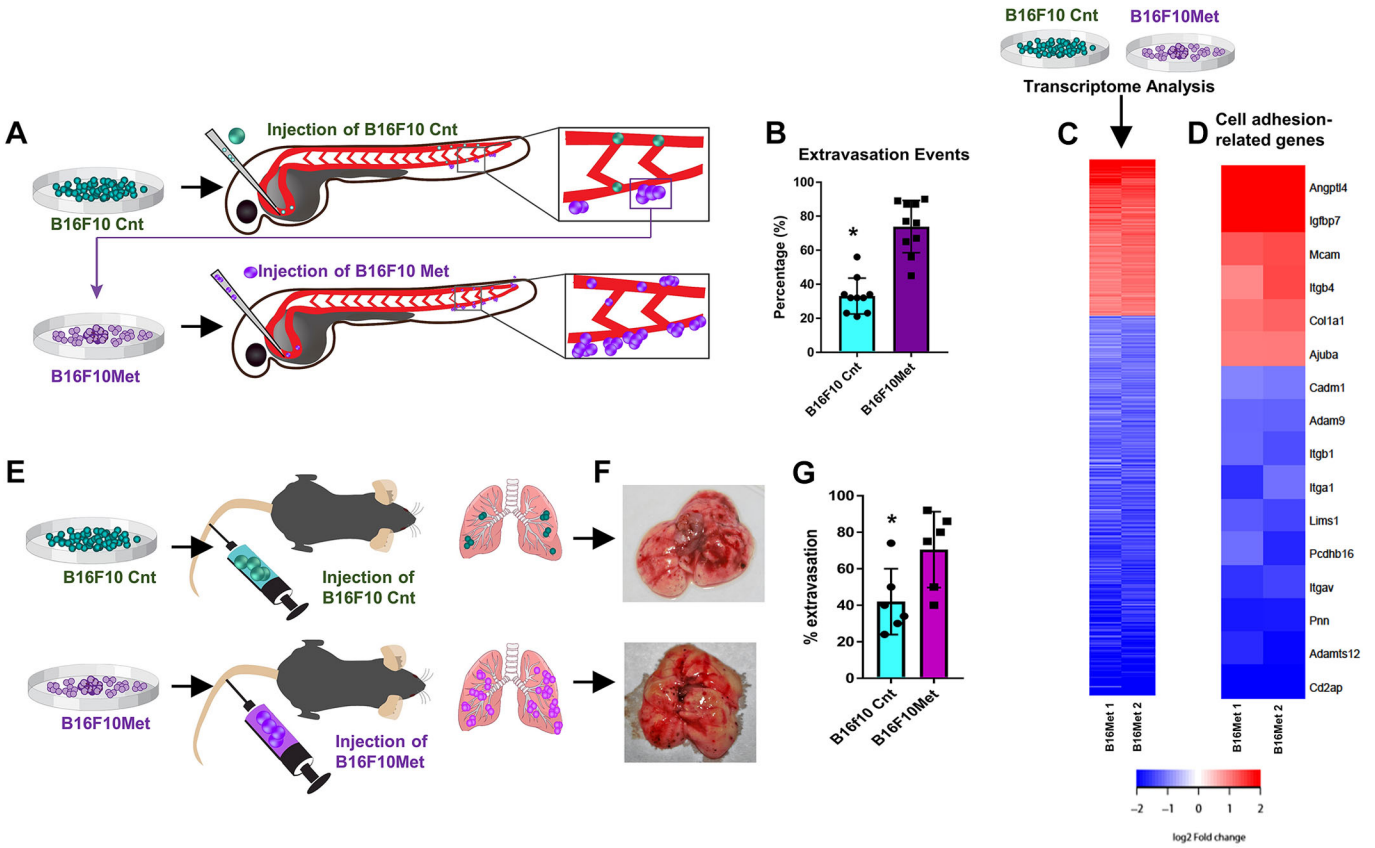

Fig. 4. Metastatic melanoma tumor cells exhibit unique gene expression profile and extravasation capability. (A,B) Illustration detailing the injection of zebrafish with B16F10 cells (Cnt) and the B16Met subline, and comparison of the percentage that extravasated. (C) Heatmap representing the differentially expressed gene (DEG) profile of B16F10 cells line isolated from extravasation-positive CTC clusters following extravasation through AP in the zebrafish model. (D) Heatmap representing a subset of cell adhesion-related DEGs of the B16F10Met cells. Red, upregulation in experimental cells compared to control; blue, downregulation in experimental cells compared to control. (E) Illustration detailing the injection of C57BL/6J with B16F10 cells and the B16Met subline. (F) Representative C57BL/6J mouse lungs 7 days post infusion of either control B16F10 cells or B16Met cells. (G) Graph representing the nodules counted on the respective mouse lungs following infusion of either B16F10 or B16Met cells (n=5). *P<0.05.

et al., 1984). Thus, is it possible that CTC clusters that maintain their adherence through the extravasation possess specific dysregulation of genes allowing them to form clusters more readily, thus giving them an advantage in proliferating following extravasation through AP.

Transcriptome analysis of CTCs sequenced immediately following AP extravasation revealed over 3000 differently expressed genes. These genes included *ZSCAN31, TRIML2, ITGA1*, *SCG5*, *NOV*, *HSPA1A* and ETS1; all of which showed significant (P<0.05) correlation between mRNA expression level and patient survival in humans. This coupled with the transcriptome data of AP-participating endothelial cells serves as a reservoir of molecular data revealing more of the complex interplay of the tumor–endothelial cell interaction during the process of metastasis and extravasation. Future studies will be needed to fully understand the whether these tumor cells exhibiting the ability to extravasate are pre-existing subsets or formed as a result of influence from the lumen/vascular microenvironment. Our results are in accordance with studies showing that increased metastatic potential correlated with tumor cell clusters in mouse models of fibrosarcoma, melanoma, and lung carcinoma (Glaves, 1983; Liotta et al., 1974).

Collectively, our study challenges current understanding that CTCs must first dissociate prior to extravasation and establishes credibility to the novel hypothesis that CTC cluster extravasate as multicellular aggregates exclusively through AP giving them a unique survival/proliferation advantage and secondary tumor formation ability (Movie 8). More specifically, our data strongly support the requirement for specific molecules to mediate the extravasation process in circulating tumor cells. Future studies on the development of drugs and therapies to target AP extravasation and CTC clusters will be of paramount in the treatment and prevention of metastasis and an enhanced knowledge of cellular extravasation through AP. The development of models to study this process with patient biopsy tissue will also be of importance and will have the potential application to offer targeted anti-metastasis treatment for cancer patients.

MATERIALS AND METHODS

Animals

All experiments involving live zebrafish and mice were performed in accordance with relevant institutional and national guidelines and regulations and were approved by the North Carolina State University Institutional Animal Care and Use Committee. For zebrafish, the transgenic lines tg(*fli1a:EGFP*) and tg(*kdrl:eosFP*) were used in this study. The resulting embryos were screened at 48 hpf for the expression of both transgenes, and double transgenic embryos were collected. In order to prevent pigmentation, 0.2 mM N-phenylthiourea (PTU; Sigma) was applied to all embryos starting at 24 hpf.

For mice, 6-week-old female C57BL/6J (Jackson Laboratories) or NOD-*scid* IL2Rg^{null} (NSG; Jackson Laboratories) were used in this study, in accordance with the NC State University-approved animal care protocol. 200 µl (3×10^5 cells) of clustered or a single-cell suspension of firefly luciferase luminescence-expressing cells were injected into a lateral tail vein of the experimental animal. At least three identical experiments were performed for each experimental set-up.

Journal of Cell Science (2019) 132, jcs231563. doi:10.1242/jcs.231563

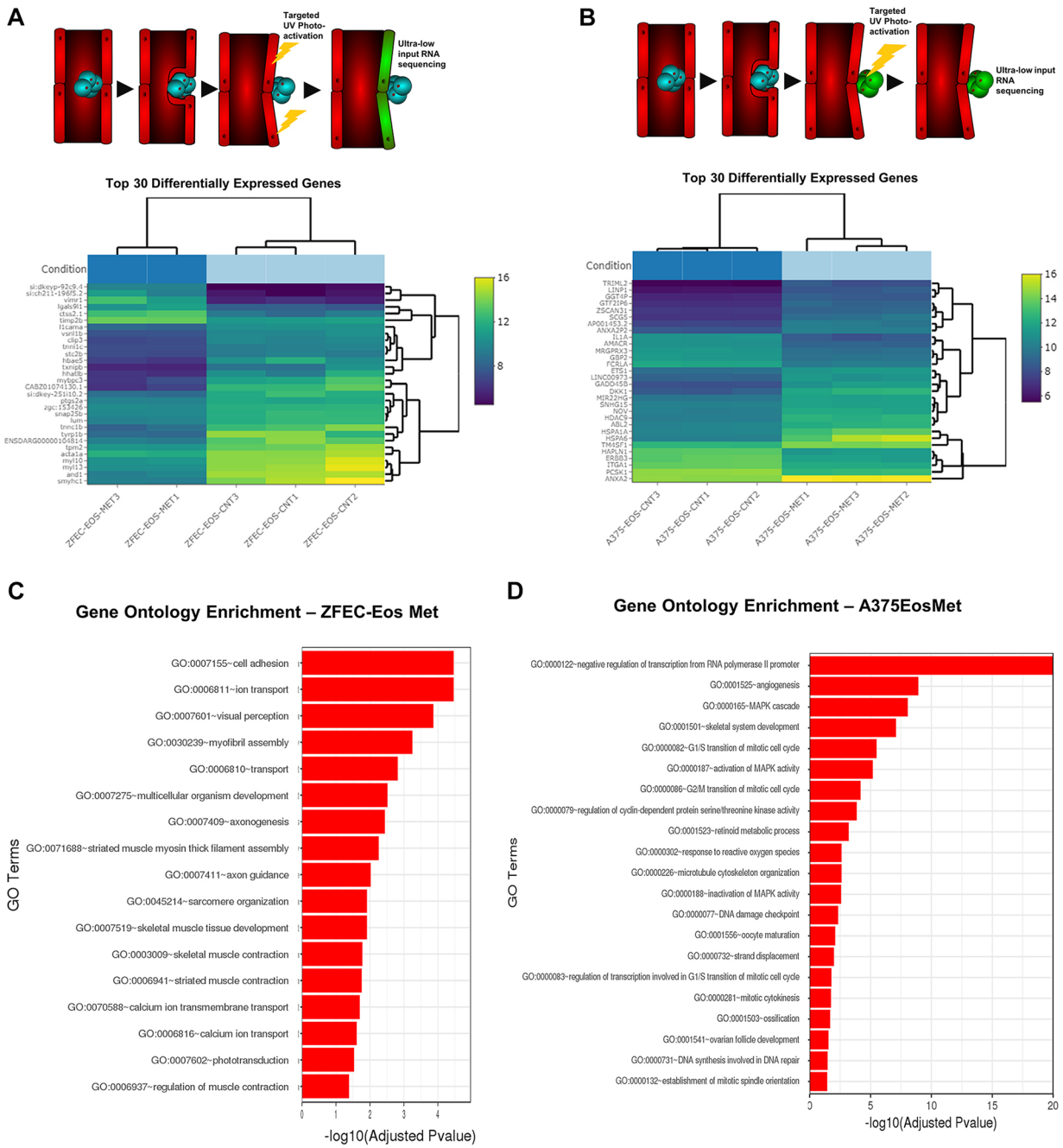

Fig. 5. Extravasation-participating endothelial and tumor cells exhibit unique genetic profiles. (A) Illustration of the photoactivation of the extravasation-participating zebrafish endothelial cells, from the tg(*kdrl:tdEos2*)*ubs15* line, following the extravasation of A375 cells; and the top 30 differentially regulated from this group. Zebrafish embryos were infused with A375 cells and immediately following extravasation through AP, endothelial cells were activated through targeted UV light at the single-cell level. Endothelial cells were sorted through FACS and pooled (500–1500 cells) for ultra-low input RNA seq (n=3). (B) Illustration of the photoactivation of the extravasation-participating zebrafish A375-EOS tumor cells, following extravasation; and the top 30 differentially regulated from this group. Zebrafish embryos were infused with A375-EOS cells and immediately following extravasation through AP, A375-EOS clusters were activated through targeted UV light at the single-cell level. Activated A375 cells were sorted through FACS and pooled (500-1500 cells) for ultra-low input RNA seq (n=3). (C,D) Significantly differentially expressed genes were clustered by their GO, and the enrichment of GO terms was tested using Fisher's exact test (GeneSCF v1.1-p2). The figures show all GO terms that are significantly enriched with an adjusted P-value less than 0.05 in the differentially expressed gene sets.

Embryo preparation and tumor cell implantation

Dechorionized 48 hpf zebrafish embryos were anaesthetized with 0.004% tricaine (Sigma) and positioned on a 200×15 mm Petri dish coated with 3% agarose. Mammalian cells were trypsinized into single-cell suspensions, resuspended in phosphate-buffered saline (PBS; Invitrogen), kept at room temperature before implantation and implanted within 2 h. Any non-fluorescent cells were labeled with the fluorescent cell tracker DiI (Invitrogen) according to the manufacturer's instructions. The cell suspension was loaded into borosilicate glass capillary needles (1 mm o.d.×0.78 mm i.d.; World Precision Instruments) and the injections were performed using a PV830 Pneumatic Pico pump and a manipulator (WPI). A total of 10–70 cells, were injected at approximately 50 µm above the ventral end of the duct of Cuvier where it opens into the heart. The approximate injection parameters were: injection pressure, 300 p.s.i.; holding pressure, 10 p.s.i.; injection time, 0.2 s. Injected tumor cells could normally be seen entering the vasculature 15–30 min after injection and starting to arrest in the vessels of the tail 1–2 h after injection.

Journal of Cell Science (2019) 132, jcs231563. doi:10.1242/jcs.231563

After implantation with mammalian cells, zebrafish embryos (including non-implanted controls) were maintained at 32°C. Normally, cell-injected embryos were euthanized at the end of experiments (~72 hpf) by tricaine overdose. For each cell line or condition, data are representative of three or more independent experiments, with five or more embryos/group. Experiments were discarded when the survival rate of the control group was <80%.

Zebrafish embryo preparation and microscopy

For live imaging in the light-sheet microscope, 48 hpf zebrafish embryos were anaesthetized using 0.016% tricaine (Sigma) and then were embedded in 1.3% low-melting-temperature agarose (Sigma; prepared in filtered fish facility water) inside a glass capillary [1.5 and 2.0 mm inner and outer diameter, respectively; 20-mm length (Zeiss)]. The embryos were centered in the capillary and oriented. After gel formation, the section of the agarose cylinder containing the tail of the embryo was extruded from the capillary by inserting wax into the capillary on the side opposite to the fish. The sample chamber of the light-sheet microscope was filled with filtered fish facility water, and the capillary was inserted for imaging. Specimens were maintained at 32°C throughout the imaging period. Fluorescence image acquisition was performed using a Zeiss Lightsheet Z.1. *z*-stacks were processed for maximum intensity projections with Zeiss ZEN software. For time-lapse (4D) images, *z*-stacks were taken every 5–15 min for a total time of up to 24 h with a step number between 50 and 200 and step size of 0.3–2.0 µm. Images were adjusted for brightness and contrast using Zeiss ZEN Software. Confirmation of injected cell migration from inside of the lumen to surrounding tissue was undertaken using the Zeiss ZEN software 3D retendering capability. Cell roundness and vascular activity was measured using ImageJ software. Vascular activity was measured by tracking multiple points of the fluorescent endothelial cells frame by frame and calculating the relative movement from one frame to another over time.

Cell culture

Human HeLa cells (ATCC, USA), murine B16-F10 melanoma cells (ATCC, USA), A375 human melanoma cells (ATCC, USA), and all other mammalian cell lines were cultured in Iscove's modified Dulbecco's medium (IMDM) with 10% (v/v) fetal bovine serum, 2 mM L-glutamine, 100 U/ml penicillin and 100 µg/ml streptomycin (all Life Technologies, Germany) at 37°C and 5% (v/v) CO_2. Primary zebrafish tumors were cultured using L-15 medium at 10% (v/v) fetal calf serum, 2 mM L-glutamine, 100 U/ml penicillin and 100 µg/ml streptomycin at 28°C. All lines were authenticated and tested negative for mycoplasma contamination. For mouse experiments with preformed clusters, the tumor cells were grown in Corning® Ultra-Low attachment cell culture flasks for 48 h prior to infusion.

Isolation and culturing of injected tumor cells from zebrafish embryos

Embryos were transferred to PBS containing 50 U/ml penicillin (Gibco) and 0.05 mg/ml streptomycin (Gibco) (PBS/PS) for at least 15 min. The PBS/PS solution was refreshed once and individual embryos were transferred to a sterile tube (embryo+500 µl PBS/PS) for 5 min. Embryos were then tranferred to 200 µl of a 1% bleaching solution for 5 min. Immediately after this, the bleaching solution was replaced with PBS/PS and incubated for 5 min, we spun down the embryos at 1200 ***g*** for 2 min at room temperature and discarded the supernatant carefully. Next, we added 300 µl of TripLE (Gibco) and incubated for 45 min at 37°C in a thermomixer, while mixing at 800 rpm. Next, we pipetted the embryo-TripLE mix with a 200-µl tip several times up and down under sterile conditions (cell culture hood) and centrifuged immediately (4 min, 1200 ***g*** at room temperature). We discarded supernatant and resuspended with 400 µl PBS and centrifuged again (4 min, 1200 ***g*** at room temperature). We resuspended the cell pellets in 200 µl growth medium and transferred the cell suspension to a 96-well plate (200 µl of medium per well).

Zebrafish primary tumor cell isolation and culture protocol

The ZF3 primary tumors were isolated from adult zebrafish from the *brca2*^{hg5} and *tp53*^{zdf1} mutant zebrafish lines carrying the *brca2*^{Q658X} and *tp53*^{M214K} mutations, respectively (Shive et al., 2010; Berghmans et al., 2005). Zebrafish were humanely euthanized with tricaine methanesulfonate (300 mg/l) in system water buffered with sodium bicarbonate to a pH of ~7.0. We isolated the tumors and placed them immediately in chilled PBS. We place a 6 mm piece of tumor in a sterile 100×20 mm plate and added 5 ml of PBS. We then cut the sample into 2 mm pieces and washed them three times with 5 ml PBS. We incubated samples in 2 ml collagenase solution at 37°C for 5 min. We then added 2 ml of L-15 medium with 15% FBS, and cut samples with blade using a rolling method until we had 50 samples roughly 0.5 mm in size. Then we placed 200 µl/well of L15 medium into 96-well plates, and added one or two pieces of 0.5 mm tumor into each well, allowing cells to attach and proliferate for several weeks. Once cells began to proliferate, we removed medium and performed a PBS wash, and trypsinized samples for 3–5 min and added medium. We then transferred the material from viable wells into a six-well plate, with 2 µl per well, and allowed cells to proliferate to confluency and then transferred them to a T-25 flask. At this point, the cells were transfected with tagRFP fluorescence using the Amaxa™ Nucleofector™ II (Lonza) and used for extravasation studies in zebrafish embryos.

RNAseq analysis of B16ZFMet cells

Total RNA was purified with an miRNeasy extraction kit (Qiagen), according to the manufacturer's guidelines, from cell pellets. RNA quality was assessed on Bioanalyzer 2100 instrument using RNA 6000 Nano Kit (Agilent). mRNA-seq sequencing libraries were prepared from 1 µg purified RNA using Illumina's TruSeq Stranded mRNA Library Prep Kit. Deep sequencing was performed on a Nextseq500 sequencer (Illumina) using 75 bp paired-end reads. Raw BCL (base call) files generated from NextSeq sequencer were converted to FASTQ files using the bcl2fastq Conversion Software v2.18. During BCL to FASTQ processing, bcl2fastq also separates multiplexed samples, removes adapters, trims low-quality bases and removes low-quality reads. Raw RNA-seq data in FASTQ file format was quality controlled during and after sequencing to identify potential technical issues. Cleaned sequencing reads were then mapped to the mouse reference genome (assembly GRCm38, Gencode annotation release M15) using STAR to generate read counts for each of annotated genes (Dobin et al., 2013). Gencode transcript annotations were supplied to facilitate the mapping of reads spanning known splicing junctions. The raw gene read count data was normalized using the voom approach (Law et al., 2014). The differential expression analysis was performed using the linear model approach provided by the limma package (Liotta et al., 1974; Ritchie et al., 2015). For the differential expression analysis, we kept only those genes with more than 30 raw read counts in at least two biological samples. The *P*-values for the coefficient/contrast of interest were adjusted for multiple testing the Benjamini and Hochberg's method (Benjamini and Hochberg, 1995), which controls the expected false discovery rate (FDR). The significance threshold for gene differential expression was defined as fold change greater than 2 and FDR less than 0.05. Raw data from RNA-seq experiment has been deposited into the Gene Expression Omnibus database as described in the Data Availability section.

Isolation of extravasation-participating endothelial cells

Fluorescent A375 tumor cells were infused into the circulation of tg(*kdrl:eosFP*) zebrafish embryos at 48 h post fertilization. Following the observation of CTC cluster extravasation through AP, the larvae were examined using intrivital microscopy to confirm the placement of the tumor cell as being outside the blood vessel lumen. Following confirmation of extravasation, targeted UV-light activation was achieved using an Olympus 471 with a focused UV penetration diameter of 10 µm. Endothelial cells were individually photoactivated for 30 s, to allow for complete transition of EosFP from GFP to RFP expression. Following activation of extravasation-participating endothelial cells, embryos were disassociated through trypsinization, as previously described in the 'Isolation and culturing of injected tumor cells from zebrafish embryos' section, and sorted through FACS directly into a Trizol solution. Photoactivated endothelial cells from ~200 embryos were pooled to a final amount of 500–1500 cells per experiment. Following sorting, cells were sent to Genewiz for ultra-low input RNA-sequencing and initial analysis.

Isolation of extravasation tumor cells

A375 tumor cells stably expressing EosFP were infused into the circulation of tg(*fli1a:EGFP*) zebrafish embryos at 48 h post fertilization. Following the

observation of CTC cluster extravasation through AP, the embryos were examined using intrivital microscopy to confirm the placement of the tumor cell as outside the blood vessel lumen. Following confirmation of extravasation, targeted UV-light activation was achieved using an Olympus 471 with a focused UV penetration diameter of 10 µm. Tumor cells were exclusively photoactivated for 30 s, to allow for complete transition of EosFP from GFP to RFP expression. Following activation of extravasation-participating tumor cells, larvae were disassociated through trypsinization, as previously described in the 'Isolation and culturing of injected tumor cells from zebrafish embryos' section, and sorted through FACS directly into a Trizol solution. Photoactiaved tumor cells from ∼200 larvae were pooled to a final amount of 500–1500 cells per experiment. Following sorting, cells were sent to Genewiz for ultra-low input RNA-sequencing and initial analysis.

Ultra-low input RNA-seq analysis

Following fluorescence activated cell sorting of either extravasation-participating tumor or endothelial cells, ultra-low input was used to sequence the cell to account for the small amounts of cells. Distribution of read counts in libraries were examined before and after normalization. The original read counts were normalized to adjust for various factors such as variations of sequencing yield between samples. These normalized read counts were used to accurately determine differentially expressed genes. Data quality assessments were performed to detect any samples that are not representative of their group, and thus, may affect the quality of the analysis. The overall similarity among samples were assessed by determining the Euclidean distance between samples. This method was used to examine which samples are similar or different to each other and if they fit to the expectation from the experiment design. The shorter the distance, the more closely related the samples are. Samples were then clustered by using the distance. Samples were projected to a 2D plane spanned by their first two principal components. Using DESeq2, a comparison of gene expression between the customer-defined groups of samples was performed. The Wald test was used to generate *P*-values and log2 fold changes. Genes with an adjusted *P*-value <0.05 and absolute log2 fold change >1 were defined as differentially expressed genes. Significantly differentially expressed genes were clustered according to their GO and the enrichment of GO terms was tested using Fisher exact test (GeneSCF v1.1-p2).

Immunohistochemistry

For immunohistochemistry (IHC) analysis of B16-F10 melanoma cells in mouse lung, tissue was fixed with 4% paraformaldehyde and permeabilized with 0.1% Triton X-100. Samples were incubated with primary anti-melanoma gp100 antibody (ab137078) at a dilution of 1:250. A goat anti-rabbit-IgG H&L (Texas Red®) (ab6719) was used as the secondary antibody at a dilution of 1:1000. For IHC analysis of endothelial tissue in mouse lung, tissue was fixed with 4% paraformaldehyde and permeabilized with 0.1% Triton X-100. Samples were incubated with primary anti-von Willebrand factor antibody (ab11713) at a dilution of 1:200. A donkey anti-sheep-IgG H&L (FITC) (ab6896) was used as the secondary antibody at a dilution of 1:1200. All antibodies were validated by Abcam.

Statistical analysis

All statistical analysis was performed using Graphpad Prism 7 (Graphpad Software, La Jolla, CA) and the Shapiro–Wilk test was performed to assess data normality. *P*-values were determined using either a Student's *t*-test (if data were normally distributed) or Mann–Whitney *U*-test (if data were not normally distributed). In figures, the bar graphs were generated using GraphPad and presented as mean±s.e.m. from at least three independent experiments. The box-and-whisker plots were generated using GraphPad in which the box ranges from 25–75th percentile, with the middle line indicating the median, and the whiskers indicating 5–95th percentile.

Acknowledgements

We thank Eva Johannes for her assistance with the light sheet microscopy, Antonio Planchart for providing the Tg(fli1a:EGFP) zebrafish line, Alice Harvey for the video animations work, the NCSU-CVM flow cytometry core Director, Javid Mohammed, for his assistance, and Dr Markus Affolter (Biozentrum University of Basel) for providing the tg(*kdrl:tdEos2*)*ubs15* zebrafish line. We also thank Genewiz for providing assistance with the ultra-low input RNA sequencing and analysis. We thank Ian Huntress for his help with figure preparation.

Competing interests

The authors declare no competing or financial interests.

Author contributions

Conceptualization: T.A.A., K.C. Methodology: T.A.A., D.A., E.A., M.T.H., J.C., A.V., P.-U.D., D.S., L.Q., T.S., S.H., H.L., E.H., C.C., X.P., J.A.Y.; Validation: T.A.A.; Formal analysis: T.A.A., A.V., J.T., P.-U.D., C.C., X.P., J.A.Y., K.C.; Investigation: T.A.A., D.A., E.A., M.T.H., J.C., L.Q.; Resources: H.S., E.H.; Data curation: T.A.A., D.A., E.A., J.C., E.H.; Writing - original draft: T.A.A.; Writing - review & editing: T.A.A., D.A., E.A., J.C., A.V., P.-U.D., L.Q., T.S., S.H., H.S., J.A.Y., K.C.; Visualization: T.A.A., T.S., S.H.; Supervision: T.A.A., J.A.Y., K.C.; Project administration: K.C.; Funding acquisition: T.A.A., K.C.

Funding

This work was supported by funding from The National Institutes of Health (HL123920 and HL137093 to K.C.) and National Cancer Institute (F31 CA217153 to T.A.A.). Deposited in PMC for release after 12 months.

Data availability

Raw files are available through the National Center for Biotechnology Information (NCBI) Gene Expression Omnibus (GEO), with accession numbers GSE132583 and GSE132082.

Supplementary information

Supplementary information available online at
http://jcs.biologists.org/lookup/doi/10.1242/jcs.231563.supplemental

References

Ablain, J. and Zon, L. I. (2013). Of fish and men: using zebrafish to fight human diseases. *Trends Cell Biol.* **23**, 584-586. doi:10.1016/j.tcb.2013.09.009

Aceto, N., Bardia, A., Miyamoto, D. T., Donaldson, M. C., Wittner, B. S., Spencer, J. A., Yu, M., Pely, A., Engstrom, A., Zhu, H. et al. (2014). Circulating tumor cell clusters are oligoclonal precursors of breast cancer metastasis. *Cell* **158**, 1110-1122. doi:10.1016/j.cell.2014.07.013

Aceto, N., Toner, M., Maheswaran, S. and Haber, D. A. (2015). En route to metastasis: circulating tumor cell clusters and epithelial-to-mesenchymal transition. *Trends Cancer* **1**, 44-52. doi:10.1016/j.trecan.2015.07.006

Allen, T. A., Gracieux, D., Talib, M., Tokarz, D. A., Hensley, M. T., Cores, J., Vandergriff, A., Tang, J., De Andrade, J. B. M., Dinh, P.-U. et al. (2017). Angiopellosis as an alternative mechanism of cell extravasation. *Stem Cells* **35**, 170-180. doi:10.1002/stem.2451

Anderson, R. L., Balasas, T., Callaghan, J., Coombe, R. C., Evans, J., Hall, J. A., Kinrade, S., Jones, D., Jones, P. S., Jones, R. et al. (2018). A framework for the development of effective anti-metastatic agents. *Nat. Rev. Clin. Oncol.* **16**, 185-204. doi:10.1038/s41571-018-0134-8

Au, S. H., Storey, B. D., Moore, J. C., Tang, Q., Chen, Y.-L., Javaid, S., Sarioglu, A. F., Sullivan, R., Madden, M. W., O'Keefe, R. et al. (2016). Clusters of circulating tumor cells traverse capillary-sized vessels. *Proc. Natl. Acad. Sci. USA* **113**, 4947-4952. doi:10.1073/pnas.1524448113

Benjamini, Y. and Hochberg, Y. (1995). Controlling the false discovery rate: a practical and powerful approach to multiple testing. *J. R. Statist. Soc. Ser. B* **57**, 289-300. doi:10.1111/j.2517-6161.1995.tb02031.x

Berghmans, S., Murphey, R. D., Wienholds, E., Neuberg, D., Kutok, J. L., Fletcher, C. D. M., Morris, J. P., Liu, T. X., Schulte-Merker, S., Kanki, J. P. et al. (2005). tp53 mutant zebrafish develop malignant peripheral nerve sheath tumors. *Proc. Natl. Acad. Sci. USA* **102**, 407-412. doi:10.1073/pnas.0406252102

Blum, Y., Belting, H.-G., Ellertsdottir, E., Herwig, L., Lüders, F. and Affolter, M. (2008). Complex cell rearrangements during intersegmental vessel sprouting and vessel fusion in the zebrafish embryo. *Dev. Biol.* **316**, 312-322. doi:10.1016/j.ydbio.2008.01.038

Bradford, Y. M., Toro, S., Ramachandran, S., Ruzicka, L., Howe, D. G., Eagle, A., Kalita, P., Martin, R., Taylor Moxon, S. A., Schaper, K. et al. (2017). Zebrafish models of human disease: gaining insight into human disease at ZFIN. *ILAR J.* **58**, 4-16. doi:10.1093/ilar/ilw040

Chávez, M. N., Aedo, G., Fierro, F. A., Allende, M. L. and Egaña, J. T. (2016). Zebrafish as an emerging model organism to study angiogenesis in development and regeneration. *Front. Physiol.* **7**, 56. doi:10.3389/fphys.2016.00056

Dobin, A., Davis, C. A., Schlesinger, F., Drenkow, J., Zaleski, C., Jha, S., Batut, P., Chaisson, M. and Gingeras, T. R. (2013). STAR: ultrafast universal RNA-seq aligner. *Bioinformatics* **29**, 15-21. doi:10.1093/bioinformatics/bts635

Duda, D. G., Duyverman, A. M. M. J., Kohno, M., Snuderl, M., Steller, E. J. A., Fukumura, D. and Jain, R. K. (2010). Malignant cells facilitate lung metastasis by bringing their own soil. *Proc. Natl. Acad. Sci. USA* **107**, 21677-21682. doi:10.1073/pnas.1016234107

Gassmann, P., Haier, J., Schlüter, K., Domikowsky, B., Wendel, C., Wiesner, U., Kubitza, R., Engers, R., Schneider, S. W., Homey, B. et al. (2009). CXCR4 regulates the early extravasation of metastatic tumor cells in vivo. *Neoplasia* **11**, 651-666. doi:10.1593/neo.09272

Gkountela, S., Castro-Giner, F., Szczerba, B. M., Vetter, M., Landin, J., Scherrer, R., Krol, I., Scheidmann, M. C., Beisel, C., Stirnimann, C. U. et al. (2019). Circulating tumor cell clustering shapes DNA methylation to enable metastasis seeding. *Cell* **176**, 98-112.e14. doi:10.1016/j.cell.2018.11.046

Glaves, D. (1983). Correlation between circulating cancer cells and incidence of metastases. *Br. J. Cancer.* **48**, 665-673. doi:10.1038/bjc.1983.248

Glinskii, O. V., Huxley, V. H., Glinsky, G. V., Pienta, K. J., Raz, A. and Glinsky, V. V. (2005). Mechanical entrapment is insufficient and intercellular adhesion is essential for metastatic cell arrest in distant organs. *Neoplasia* **7**, 522-527. doi:10.1593/neo.04646

Gore, A. V., Monzo, K., Cha, Y. R., Pan, W. and Weinstein, B. M. (2012). Vascular development in the zebrafish. *Cold Spring Harb. Perspect. Med.* **2**, a006684. doi:10.1101/cshperspect.a006684

Gundem, G., Perez-Llamas, C., Jene-Sanz, A., Kedzierska, A., Islam, A., Deu-Pons, J., Furney, S. J. and Lopez-Bigas, N. (2010). IntOGen: Integration and data mining of multidimensional oncogenomic data. *Nat. Methods* **7**, 92-93. doi:10.1038/nmeth0210-92

Hou, J.-M., Krebs, M., Ward, T., Sloane, R., Priest, L., Hughes, A., Clack, G., Ranson, M., Blackhall, F. and Dive, C. (2011). Circulating tumor cells as a window on metastasis biology in lung cancer. *Am. J. Pathol.* **178**, 989-996. doi:10.1016/j.ajpath.2010.12.003

Huang, M.-Y., Tsai, H.-L., Huang, J.-J. and Wang, J.-Y. (2016). Clinical implications and future perspectives of circulating tumor cells and biomarkers in clinical outcomes of colorectal cancer. *Transl. Oncol.* **9**, 340-347. doi:10.1016/j.tranon.2016.06.006

Law, C. W., Chen, Y., Shi, W. and Smyth, G. K. (2014). voom: Precision weights unlock linear model analysis tools for RNA-seq read counts. *Genome Biol.* **15**, R29. doi:10.1186/gb-2014-15-2-r29

Lenard, A. N., Ellertsdóttir, E., Herwig, L., Krudewig, A., Sauteur, L., Belting, H.-G. and Affolter, M. (2013). In vivo analysis reveals a highly stereotypic morphogenetic pathway of vascular anastomosis. *Dev. Cell* **25**, 492-506. doi:10.1016/j.devcel.2013.05.010

Liotta, L. A., Kleinerman, J. and Saidel, G. M. (1974). Quantitative relationships of intravascular tumor cells, tumor vessels, and pulmonary metastases following tumor implantation. *Cancer Res.* **34**, 997-1004.

Miles, F. L., Pruitt, F. L., Van Golen, K. L. and Cooper, C. R. (2008). Stepping out of the flow: capillary extravasation in cancer metastasis. *Clin. Exp. Metastasis* **25**, 305-324. doi:10.1007/s10585-007-9098-2

Ritchie, M. E., Phipson, B., Wu, D., Hu, Y., Law, C. W., Shi, W. and Smyth, G. K. (2015). limma powers differential expression analyses for RNA-sequencing and microarray studies. *Nucleic Acids Res.* **43**, e47. doi:10.1093/nar/gkv007

Shive, H. R., West, R. R., Embree, L. J., Azuma, M., Sood, R., Liu, P. and Hickstein, D. D. (2010). brca2 in zebrafish ovarian development, spermatogenesis, and tumorigenesis. *Proc. Natl. Acad. Sci. USA* **107**, 19350-19355. doi:10.1073/pnas.1011630107

Stott, S. L., Hsu, C.-H., Tsukrov, D. I., Yu, M., Miyamoto, D. T., Waltman, B. A., Rothenberg, S. M., Shah, A. M., Smas, M. E., Korir, G. K. et al. (2010). Isolation of circulating tumor cells using a microvortex-generating herringbone-chip. *Proc. Natl. Acad. Sci. USA* **107**, 18392-18397. doi:10.1073/pnas.1012539107

Strell, C. and Entschladen, F. (2008). Extravasation of leukocytes in comparison to tumor cells. *Cell Commun. Signal.* **6**, 10. doi:10.1186/1478-811X-6-10

Taddei, M. L., Giannoni, E., Fiaschi, T. and Chiarugi, P. (2012). Anoikis: an emerging hallmark in health and diseases. *J. Pathol.* **226**, 380-393. doi:10.1002/path.3000

Updyke, T. V. and Nicolson, G. L. (1986). Malignant melanoma cell lines selected in vitro for increased homotypic adhesion properties have increased experimental metastatic potential. *Clin. Exp. Metast.* **4**, 273. doi:10.1007/BF00133592

Urushihara, H., Ikawa, Y. and Tsuruo, T. (1984). Adhesive properties of weakly and highly metastatic melanoma cell lines. *Gann* **75**, 534-539.